Fragile charge order in the non-superconducting ground state of the underdoped high temperature superconductors

B. S. Tan[1], N. Harrison[2], Z. Zhu[2], F. F. Balakirev[2], B. J. Ramshaw[2], A. Srivastava[1],
S. A. Sabok[3], B. Dabrowski[3], G. G. Lonzarich[1], and Suchitra E. Sebastian[1]

[1] *Cavendish Laboratory, Cambridge University, JJ Thomson Avenue, Cambridge CB3 0HE, U.K*
[2] *National High Magnetic Field Laboratory, LANL, Los Alamos, NM 87545*
[3] *Physics Department, Northern Illinois University, DeKalb, Illinois 60115*
(Dated: April 2, 2015)

The normal state in the hole underdoped copper oxide superconductors has proven to be a source of mystery for decades. The measurement of a small Fermi surface by quantum oscillations on suppression of superconductivity by high applied magnetic fields, together with complementary spectroscopic measurements in the hole underdoped copper oxide superconductors, reveals a nodal electron pocket from charge order in $YBa_2Cu_3O_{6+\delta}$. Here we report quantum oscillation measurements in the closely related stoichiometric material $YBa_2Cu_4O_8$, which reveal similar Fermi surface properties to $YBa_2Cu_3O_{6+\delta}$, despite an absence of charge order signatures in the same spectroscopic techniques such as x-ray diffraction that revealed signatures of charge order in $YBa_2Cu_3O_{6+\delta}$. Fermi surface reconstruction in $YBa_2Cu_4O_8$ is suggested to occur from magnetic field enhancement of charge order that is rendered fragile in zero magnetic fields due to its potential unconventional symmetry, and/or its occurring as a subsidiary to more robust underlying electronic correlations.

PACS numbers: 71.45.Lr, 71.20.Ps, 71.18.+y

Significance

Quantum oscillation experiments have suggested charge order as responsible for the creation of a nodal electron pocket in the $YBa_2Cu_3O_{6+\delta}$ and $HgBa_2CuO_{4+\delta}$ families of underdoped cuprates. Yet the situation in the pristine $YBa_2Cu_4O_8$ family remains ambiguous, calling into question this finding. Our high precision quantum oscillation measurements reveal a very similar nodal electron pocket in the stoichiometric cuprate family $YBa_2Cu_4O_8$ despite the non-observation of charge order by diffraction experiments. Our findings associate the mysteriously short correlation length of charge order in low magnetic fields with impurity pinning in other families of cuprates, and suggest an origin of fragile charge order either from an unconventional symmetry of the order parameter, and/or its subsidiary role to a more robust primary order parameter.

Introduction

The normal state of the underdoped copper oxide superconductors has proven to be even more perplexing than the d-wave superconducting state in these materials. At high temperatures in zero magnetic fields, the normal state of the underdoped cuprates comprises an unconventional Fermi surface of truncated 'Fermi arcs' in momentum space, referred to as the pseudogap state [1]. At low temperatures in high magnetic fields, quantum oscillations reveal the non-superconducting ground state in various families of underdoped hole-doped copper-oxide

superconductors to comprise small Fermi surface pockets [2–15]. These small Fermi pockets in $YBa_2Cu_3O_{6+\delta}$ have been identified as nodal electron pockets [2, 3, 11, 16, 17] originating from Fermi surface reconstruction associated with charge order measured by x-ray diffraction [18–20], ultrasound [21], nuclear magnetic resonance [22], and optical reflectometry [23]. Yet various aspects of the underlying charge order and the associated Fermi surface reconstruction remains obscure. A central question pertains to the origin of this charge order, curious features of which include a short correlation length in zero magnetic field that grows with increasing magnetic field and decreasing temperature [20]. It is crucial to understand the nature of this ground state order that is related to the high temperature pseudogap state, and is delicately balanced with the superconducting ground state. Here we shed light on the nature of this state by performing extended magnetic field, temperature, and tilt angle-resolved quantum oscillation experiments in the stoichiometric copper-oxide superconductor $YBa_2Cu_4O_8$ [24]. This material with double CuO chains has fixed oxygen stoichiometry, making it a model system to study. $YBa_2Cu_4O_8$ avoids disorder associated with the fractional oxygen stoichiometry in the $YBa_2Cu_3O_{6+\delta}$ chains which has been shown by microwave conductivity to be the dominant source of weak-limit (Born) scattering [25].

Intriguingly, we find magnetic field and angle-dependent signatures of quantum oscillations in $YBa_2Cu_4O_8$ [13, 14] that are very similar to those in $YBa_2Cu_3O_{6+\delta}$, indicating a similar Fermi surface comprising a nodal electron pocket that arises from Fermi

surface reconstruction by charge order [16]. Yet the same x-ray diffraction measurements that show a Bragg peak characteristic of charge order in $YBa_2Cu_3O_{6+\delta}$ for a range of hole dopings from $0.084 \leq p \leq 0.164$ [19, 20, 26] reveal a notable absence of a Bragg peak in the case of $YBa_2Cu_4O_8$ (Fig. 3 in ref. [19]). We suggest that charge order enhanced by applied magnetic fields reconstructs the Fermi surface in $YBa_2Cu_4O_8$, while charge order is revealed even in zero magnetic fields in $YBa_2Cu_3O_{6+\delta}$ due to pinning by increased disorder from oxygen vacancies.

Results

Fig. 1 shows quantum oscillations in contactless conductivity [27] measured up to 90 T in $YBa_2Cu_4O_8$ and at different temperatures from 1.3 K to 8.0 K. The extended magnetic field range and increased sensitivity compared to previous quantum oscillation experiments [13, 14] enables precision measurements of the quantum oscillation frequency spectrum and effective quasiparticle mass of $YBa_2Cu_4O_8$.

Preliminary quantum oscillation measurements on $YBa_2Cu_4O_8$ accessed two [13] to four [14] oscillation periods over a restricted magnetic field range, for a magnetic field angle parallel to the crystalline $\hat{c}$-axis. A single quantum oscillation frequency of 660(30) T was reported, while the scatter of the quantum oscillation amplitude as a function of temperature precluded a determination as to whether a Lifshitz-Kosevich form is obeyed or an accurate extraction of a quasiparticle effective mass. Our present quantum oscillation measurements over an extended magnetic field range access more than seven oscillation periods, revealing for the first time a pronounced quantum oscillation beat structure characteristic of multiple frequencies, very similar to $YBa_2Cu_3O_{6.56}$ [6, 9, 31], with a dominant frequency of 640 T. Our precision measurements of quantum oscillation amplitude as a function of temperature shown in Fig. 1b,c further reveal a distinctive Lifshitz Kosevich form, characteristic of Fermi Dirac statistics. A fit to the Lifshitz Kosevich form yields a quasiparticle effective mass of $1.8(1)m_e$ in $YBa_2Cu_4O_8$, which is in fact very similar to that measured for $YBa_2Cu_3O_{6.56}$.

Angular measurements as a function of tilt angle to the applied magnetic field are required in order to identify the origin of the multiple frequency spectrum we observe in $YBa_2Cu_4O_8$. Fig. 2 shows the quantum oscillations in $YBa_2Cu_4O_8$ measured up to a maximum tilt angle of $\theta \approx 56°$. A few key features are notable. Firstly, the beat pattern at the zero degree tilt angle persists up to high tilt angles. Secondly, the prominent Yamaji amplitude resonance [28] expected at $\theta \approx 52°$ for a neck-belly warped Fermi surface in $YBa_2Cu_4O_8$ is absent up to the measured high tilt angles. The absence of a prominent
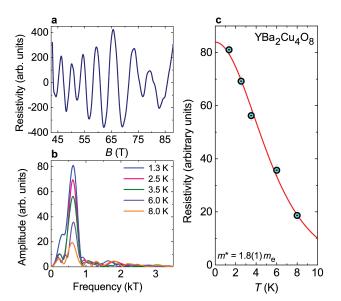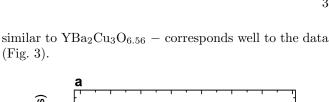

FIG. 1: (a) Quantum oscillations measured in the contactless resistivity of $YBa_2Cu_4O_8$ for the magnetic field parallel to c-axis, (b) Fourier transform of the measured quantum oscillations at different temperatures, (c) plot of quantum oscillation amplitude as a function of temperature (symbols) accompanied by a Lifshitz Kosevich fit (red line).

Yamaji angle in $YBa_2Cu_4O_8$ enables us to rule out a Fermi surface where the observed frequency spread arises from a dominant neck and belly fundamental warping. Instead, both the observed features are consistent with a quasi-two dimensional Fermi surface in which the multiple frequency spectrum originates from a splitting of frequencies as opposed to a fundamental neck and belly warping. Such a quasi-two dimensional Fermi surface is similar to that identified in $YBa_2Cu_3O_{6+\delta}$ [16, 31].

A further clue as to the origin of the observed quantum oscillations in $YBa_2Cu_4O_8$ is obtained by inspecting the evolution of the amplitude and phase of the quantum oscillations as a function of tilt angle. Fig. 3b shows the cross-correlation function between the measured quantum oscillations in $YBa_2Cu_4O_8$ and a phase-matched sinusoidal function with frequency 640 T, which is averaged over the indicated magnetic field range, referred to as the correlator. We find that the correlator is very similar to that previously measured for the $YBa_2Cu_3O_{6.56}$ [11, 16] and shown in Fig. 3a. The correlator for $YBa_2Cu_4O_8$ reveals a zero crossing and phase inversion of the quantum oscillation amplitude signalling a spin zero at a tilt angle of $\theta \approx 48°$. A 'spin zero' feature arises on destructive interference between quantum oscillations from two spin channels at certain special angles. At these spin zero angles, the ratio of the Zeeman energy to the cyclotron energy — captured by the spin splitting factor $R_s = \cos\left[\frac{\pi}{2}\frac{m_\parallel^* g_\parallel^*}{m_e \cos\theta}\right]$ — crosses zero, and

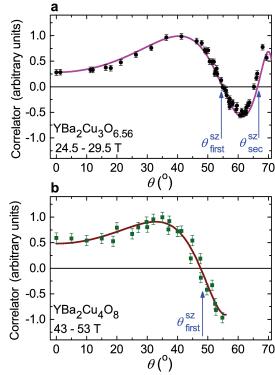FIG. 2: Quantum oscillations (in colour) measured in the contactless resistivity of $YBa_2Cu_4O_8$ for different angles of inclination (θ) of the magnetic field to the c-axis plotted as a function of $B\cos\theta$. Simulated quantum oscillations (in gray) of a bilayer split quasi-two dimensional Fermi surface model shown in Fig. 4 [16] for parameters listed in Table I. The inset shows a schematic of the crystal tilt angle to the magnetic field.

similar to $YBa_2Cu_3O_{6.56}$ − corresponds well to the data (Fig. 3).

FIG. 3: **a** Symbols represent the cross-correlation function between the measured quantum oscillations in $YBa_2Cu_3O_{6.56}$ and a phase-matched sinusoidal function with frequency 534 T, which is averaged over the indicated magnetic field range (data from ref. [16]). **b** Symbols represent the cross-correlation function between the measured quantum oscillations in $YBa_2Cu_4O_8$ and a phase-matched sinusoidal function with frequency 640 T, which is averaged over the indicated experimental magnetic field range. Solid lines in **a** and **b** show the fits using the equation and parameters in Table I.

inverts sign. Spin zero angles are located at

$$\theta_{sz} = \cos^{-1}\left[\frac{m_{\parallel}^* g_{\parallel}^*}{(2n+1)m_e}\right], \tag{1}$$

where n is an integer, $g_{\parallel}^*$ is the effective g-factor for B parallel to the crystalline $\hat{c}$-axis, m_e is the electron mass, and $m_{\parallel}^*$ is the effective quasiparticle mass for B parallel to the crystalline $\hat{c}$-axis [30].

A value of $m_{\parallel}^* g_{\parallel}^*$ can be extracted by the measurement of at least two spin zeros, given the two unknown quantities n and $g_{\parallel}^*$, as was done the case of $YBa_2Cu_3O_{6.56}$ [16]. To interpret the single spin zero in $YBa_2Cu_4O_8$, a comparison with $YBa_2Cu_3O_{6.56}$ is instructive, in which case a value of $n = 2$ for the first spin zero and $m_{\parallel}^* g_{\parallel}^* \approx 3.4$ for the dominant frequency yielded good agreement with the two observed spin zeros at $\theta_{first}^{sz} \approx 55°$ [10, 16] and $\theta_{sec}^{sz} \approx 66°$ [16]. In the case of $YBa_2Cu_4O_8$, an association of a value of $n = 2$ for the first observed spin zero at $\theta_{first}^{sz} \approx 48°$ and a value of $m_{\parallel}^* g_{\parallel}^* \approx 3.6$ for the dominant frequency (denoted by subscript $\square$ in Table I) − very

Given the similarities we find between $YBa_2Cu_4O_8$ and $YBa_2Cu_3O_{6+\delta}$ in terms of the measured multiple quantum oscillation frequency spectrum, split quasi-two dimensional Fermi surface, and spin zero angles revealed by the correlator, we compare the measured quantum oscillations in $YBa_2Cu_4O_8$ with the Fermi surface model fit to the measured quantum oscillations in $YBa_2Cu_3O_{6+\delta}$ [11, 16, 17]. We consider a model in which cyclotron orbits are associated with a nodal bilayer split Fermi surface from charge ordering shown in Fig. 4. Here the quantum oscillation frequency spread is associated with a splitting of the Fermi surface arising from tunnelling between bilayers. Magnetic breakdown tunnelling in the nodal region where the splitting is smallest can then give rise to a series of combination frequencies, as discussed in refs. [16, 31]. Fig. 2, 3 shows that this model can simulate the angular and magnetic field dependence of the quantum oscillations measured in $YBa_2Cu_4O_8$ reasonably well. The parameters

parameter	description	YBa$_2$Cu$_4$O$_8$	YBa$_2$Cu$_3$O$_{6.56}$
F_0	quantum oscillation frequency	639 T	534 T
$\Delta F_{\text{twofold}}$	staggered twofold warping frequency	–	15 T
ΔF_{split}	bilayer splitting frequency	91 T	90 T
$m_{\parallel}^*$	quasiparticle effective mass	1.8 m_e (fixed)	1.6 m_e (fixed)
B_0	magnetic breakdown field	4.2 T	2.7 T
$g_{\parallel\square}^*$	g-factor 1	2.0	2.1
$g_{\parallel\diamond}^*$	g-factor 2	0.1	0.4
$\xi_\square$	g-factor anisotropy 1	1.6	1.4
$\xi_\diamond$	g-factor anisotropy 2	0.8	0.2
ϕ	phase	-1.6	0 (fixed)

TABLE I: Parameters used to simulate the oscillatory waveform for a quasi-two dimensional split Fermi surface model shown in Fig. 4, represented by the Eqn. $\Psi_{\text{twofold}} \approx \sum_{j=1}^{6} N_j [R_{\text{MB}} R_s R_D R_T]_j \cos\left(\frac{2\pi F_j}{B\cos\theta} - \pi + \phi\right)$. Here, R_{MB} is the magnetic breakdown amplitude reduction factor (defined in the methods section), and N_j counts the number of instances the same orbit is repeated within the magnetic breakdown network. R_D is the Dingle damping factor, R_T is the thermal damping factor, R_s is the spin damping factor (defined in the methods section). The tabulated values used to simulate the quantum oscillation waveform yield good agreement with experiment as a function of B and θ (Fig. 2, 3). The effective mass is taken to be a fixed quantity, having been determined independently from temperature-dependent measurements [9]. The parameters are the same for all the orbits, except for those denoted by subscripts $\square$ and $\diamond$, which each correspond to a subset of orbits as defined in the text. The values of $g_{\parallel j}^*$ and ξ_j here represent parameters used for the simulation rather than unique identifications. The parameters used for YBa$_2$Cu$_3$O$_{6.56}$ shown for comparison are taken from ref. [16].
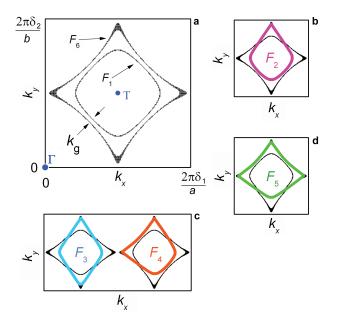

FIG. 4: Brillouin zone cross section, showing a schematic of a nodal electron pocket created by charge ordering wavevectors $\mathbf{Q}_1 = 2\pi(\pm\frac{\delta_1}{a}, 0, \pm\frac{1}{2c})$ and $\mathbf{Q}_2 = 2\pi(0, \pm\frac{\delta_2}{b}, \pm\frac{1}{2c})$ [11, 16, 17]. **a** shows the two Fermi surface cross-sections of frequency $F_1 = F_0 - 2\Delta F_{\text{split}}$ and $F_6 = F_0 + 2\Delta F_{\text{split}}$. The gap separating bonding and antibonding surfaces is expected to be smallest at the nodes [29]. A cut through the $k_z = 0$ plane of the Brillouin zone shows the possible magnetic breakdown orbits [16, 31]. **b**, **c**, **d** and **e** show the range of possible magnetic breakdown orbits, $F_2 = F_0 - \Delta F_{\text{split}}$, $F_3 = F_0$, $F_4 = F_0$ and $F_5 = F_0 + \Delta F_{\text{split}}$, as listed in Table I.

used for the model simulation are in fact very similar to those used to simulate quantum oscillations measured in YBa$_2$Cu$_3$O$_{6.56}$ (Table I) [16]. The small staggered twofold warping included in the case of YBa$_2$Cu$_3$O$_{6.56}$ is not included for YBa$_2$Cu$_4$O$_8$, given the restricted angular range over which quantum oscillations can be accessed, and the likely weaker amplitude warping associated with a longer c-axis. We note there is some deviation from the model at a few of the highest angles. This may be due to a further lifting of degeneracy of frequency components from effects such as a distortion of the simple tetragonal crystal structure or other details of Fermi surface geometry beyond those considered in the present model.

Discussion

Our findings therefore reveal closely similar quantum oscillation features in YBa$_2$Cu$_4$O$_8$ compared to YBa$_2$Cu$_3$O$_{6.56}$, showing (i) a similar quasiparticle effective mass from a Lifshitz Kosevich fit to the amplitude dependence as a function of temperature, (ii) a spread of multiple frequencies yielding a prominent beat structure, (iii) an angular dependence of quantum oscillation frequencies consistent with Fermi surface splitting accompanied by magnetic breakdown, rather than fundamental neck and belly warping, (iv) a similar value of m^*g^* from the angular dependence and 'spin zero' observed in the correlator. The common Fermi surface features point to the same origin of Fermi surface reconstruction in YBa$_2$Cu$_4$O$_8$ as in YBa$_2$Cu$_3$O$_{6+\delta}$.

In the case of YBa$_2$Cu$_3$O$_{6+\delta}$, the electronic struc-

ture comprises a nodal electron pocket associated with Fermi surface reconstruction by a superstructure with orthogonal wavevectors $\mathbf{Q}_1 = 2\pi(\pm\frac{\delta_1}{a}, 0, \pm\frac{1}{2c})$ and $\mathbf{Q}_2 = 2\pi(0, \pm\frac{\delta_2}{b}, \pm\frac{1}{2c})$ associated with charge order observed by x-ray diffraction and other experiments (where $\delta_1 \approx \delta_2 \approx 0.3$) [19, 20, 22]. Given the similarity of quantum oscillation features in $YBa_2Cu_4O_8$ measurements, the lack of charge order detected by various measurement techniques in this material (e.g. x-ray diffraction results in Fig. 3 of ref. [19]) is striking.

An unusual aspect of the charge order measured in $YBa_2Cu_3O_{6+\delta}$ is the short average correlation length, which has been measured to be of the order of 100 $\mathring{A}$ from x-ray diffraction measurements in a magnetic field of 17 T [20]. The measured average correlation length is comparable with the cyclotron radius of $100 - 200$ $\mathring{A}$ in the magnetic field range $30 - 100$ T where quantum oscillations are measured [2–12], consistent with the notion that Fermi surface reconstruction may be observed by quantum oscillation measurements for correlations that are of wavelength longer than the cyclotron radius and frequency slower than the cyclotron frequency. It has remained unclear thus far, however, whether the short correlation length is due to the nucleation and pinning of charge order at impurity/defect sites, or whether it is due to the disruptive effects of impurities/defects in an intrinsically long range charge ordered state [32, 33]

Our findings in $YBa_2Cu_4O_8$, where impurity pinning centres are reduced compared to $YBa_2Cu_3O_{6+\delta}$ due to the fixed oxygen stoichiometry, suggest that charge order of inherently short correlation length arises in zero magnetic fields in $YBa_2Cu_3O_{6+\delta}$ on account of impurity sites that act as pinning potential centres. Charge order in the well-known charge ordered material $NbSe_2$ has, for instance, been shown to initially develop around impurities [34]. In the case of $YBa_2Cu_4O_8$, however, where such impurity pinning centres are reduced, applied magnetic fields are required to tilt the balance of energy scales such that charge susceptibility is further enhanced, and charge order is revealed to reconstruct the Fermi surface.

Our findings point to a fragile form of charge order in the non-superconducting ground state of the underdoped cuprates which is enhanced by applied magnetic fields to yield Fermi surface reconstruction. An interesting question pertains to the origin of such intrinsically fragile charge order. A contributing factor may be the potential d-wave rather than the more conventional s-wave symmetric form factor of these charge correlations [35]. Further, charge order may arise as a corollary to more robust correlations in the underdoped cuprates, such as underlying strong spin correlations [36]. The interplay between these correlations may be manifested as other order parameters such as Amperean order [37], pair density wave order [38], d-wave checkerboard order [39], and quadrupolar order [40, 41], which have also been proposed to appear in fluctuating form above the superconducting temperature.

Methods

Quantum oscillation simulations include conventional thermal, Dingle, and spin damping factors of the same form used for previous comparisons with quantum oscillations measured in the underdoped cuprates and other layered families of materials [30].

The thermal damping factor is given by

$$R_T = \frac{X_j}{\sinh X_j}$$

(where $X_j = 2\pi^2 k_B m_{\theta j}^* T/\hbar e B \cos\theta$), k_B is the Boltzmann factor, T is the temperature, $m_{\theta j}^* = m_{\|j}^*/\cos\theta$ (taken to be the same for all orbits and the subscript 'j' dropped) is determined by the projection $B\cos\theta$ of B perpendicular to the planes (i.e. the projection parallel to the $\hat{c}$-axis in $YBa_2Cu_3O_{6+x}$). $m_{\|j}^*$ refers to the value of $m_{\theta j}^*$ when B is parallel to the crystalline $\hat{c}$-axis (taken to be a fixed quantity, determined independently from temperature-dependence measurements [9]).

The Dingle damping factor is given by

$$R_D = \exp\left(-\frac{\Lambda_j}{B\cos\theta}\right),$$

(where Λ_j is a damping factor, taken to be the same for all orbits, enabling us to drop the subscript j) [30].

The spin damping factor is given by

$$R_s = \cos\left[\frac{\pi}{2}\left(\frac{m_{\theta j}^*}{m_e}\right)g_{\theta j}^*\right],$$

where the anisotropic effective g-factor has the form $g_{\theta j}^* = g_{\parallel j}^* \sqrt{\cos^2 \theta + \frac{1}{\xi_j} \sin^2 \theta}$. Here, $g_{\parallel j}^*$ refers to the value of $g_{\theta j}^*$ when B is parallel to the crystalline $\hat{c}$-axis, while $\xi_j = \left(\frac{g_\parallel^*}{g_\perp^*}\right)^2$ is the anisotropy in the spin susceptibility. Two sets of anistropic g-factors are considered for subsets of orbits defined below. Because of the multiple frequencies in the model and the restricted angular range measured, it is not possible to uniquely identify the g-factors. The values of $g_{\parallel j}^*$ and ξ_j here represent parameters used for the simulation.

A splitting of the Fermi surface arising from tunnelling between bilayers leads to two starting frequencies that are denoted as $F_1 = F_0 - 2F_{\text{split}}$ and $F_6 = F_0 + 2F_{\text{split}}$. Magnetic breakdown tunnelling (in the nodal region where the splitting is smallest) gives rise to a series of combination frequencies F_2, F_3, F_4, F_5, as discussed in refs. [16, 31]. Only two sets of anisotropic g-factors are considered: orbits F_1, F_2, F_4, F_5 and F_6, which undergo both magnetic breakdown tunnelling and finite Bragg reflection are approximated to have the same g-factor $g_{\parallel \diamond}^*$ with anisotropy $\xi_\diamond$, while orbits F_3, which show only magnetic breakdown tunnelling without finite Bragg reflection are approximated to have a common g-factor $g_{\parallel \square}^*$ with anisotropy $\xi_\square$ [16]. The magnetic breakdown amplitude reduction factor is given by

$$R_{\text{MB}} = (i\sqrt{P})^{l_\nu}(\sqrt{1-P})^{l_\eta},$$

in which l_ν and l_η count the number of magnetic breakdown tunnelling and Bragg reflection events *en route* around the orbit, having transmitted amplitudes $i\sqrt{P}$ and $\sqrt{1-P}$ respectively. The magnetic breakdown probability is given by $P = \exp(-B_0/B\cos\theta)$, where B_0 is the characteristic magnetic breakdown field [30].

---

[1] Timusk, T. and Statt, B. The pseudogap in high-temperature superconductors: an experimental survey. Rep. Prog. Phys. **62**, 61 (1999).

[2] Doiron-Leyraud, N. *et al.* Quantum oscillations and the Fermi surface in an underdoped high-T_c superconductor. Nature **447**, 565 (2007).

[3] LeBoeuf, D. *et al.* Electron pockets in the Fermi surface of hole-doped high-T_c superconductors. Nature **450**, 533 (2007).

[4] Jaudet, C. *et al.* de Haas-van Alphen oscillations in the underdoped high-temperature superconductor YBa$_2$Cu$_3$O$_{6.5}$. Phys. Rev. Lett. **100**, 187005 (2008).

[5] Sebastian, S. E. *et al.* Multi-component Fermi surface in an underdoped high temperature superconductor. Nature **454**, 200 (2008).

[6] Audouard, A. *et al.* Multiple frequencies in quantum oscillations from underdoped YBa$_2$Cu$_3$O$_{6.5}$. Phys. Rev. Lett. **103**, 157003 (2009).

[7] Sebastian, S. E. *et al.* Fermi-liquid behavior in an underdoped high-T_c superconductor. Phys. Rev. B **81**, 140505(R) (2010).

[8] Singleton, J. *et al.* Magnetic Quantum Oscillations in YBa$_2$Cu$_3$O$_{6.61}$ and YBa$_2$Cu$_3$O$_{6.69}$ in Fields of Up to 85 T: Patching the Hole in the Roof of the Superconducting Dome. Phys. Rev. Lett. **104**, 086403 (2010).

[9] Sebastian, S. E. *et al.* Compensated electron and hole pockets in an underdoped high-T_c superconductor. Phys. Rev. B **81**, 214524 (2010).

[10] Ramshaw, B. J. *et al.* Angle dependence of quantum oscillations in YBa$_2$Cu$_3$O$_{6.59}$ shows free-spin behaviour of quasiparticles. Nature Phys. **7**, 234-238 (2011).

[11] Sebastian, S. E., Harrison, N. & Lonzarich, G. G. Towards resolution of the Fermi surface in underdoped high-T_c superconductors. Rep. Prog. Phys. **75**, 102501 (2012).

[12] Riggs, S. C. *et al.* Heat capacity through the magnetic-field-induced resistive transition in an underdoped high-temperature superconductor. Nature Phys. **7**, 332-335 (2011).

[13] Bangura, A. F. *et al.* Small Fermi surface pockets in underdoped cuprate superconductors: Shubnikov-de Haas oscillations in YBa$_2$Cu$_4$O$_8$. Phys. Rev. Lett. **100**, 047004 (2008).

[14] Yelland, E. A. *et al.* Quantum oscillations in the underdoped cuprate YBa$_2$Cu$_4$O$_8$. Phys. Rev. Lett. **100**, 047003 (2008).

[15] Barisic, N. *et al.* Universal quantum oscillations in the underdoped cuprate superconductors. Nature Phys. **9**, 761-764 (2013).

[16] Sebastian, S.E. *et al.* Normal-state nodal electronic structure in underdoped high-T_c copper oxides. Nature **511**, 61-64 (2014).

[17] Harrison N. & Sebastian, S. E., Protected Nodal Electron Pocket from Multiple-Q Ordering in Underdoped High Temperature Superconductors. Phys. Rev. Lett. **106**, 226402 (2011).

[18] Tabis, W. *et al.* Charge order and its connection with Fermi-liquid charge transport in a pristine high-T_c cuprate. Nature Commun. **5**, 5875 (2014).

[19] Ghiringhelli, G. *et al.* Long-range incommensurate charge fluctuations in (Y,Nd)Ba$_2$Cu$_3$O$_{6+x}$. Science **337**, 821-825 (2012).

[20] Chang, J. *et al.* Direct observation of competition between superconductivity and charge density wave order in YBa$_2$Cu$_3$O$_{6.67}$. Nature Phys. **8**, 871-876 (2012).

[21] LeBoeuf, D. *et al.* Thermodynamic phase diagram of static charge order in underdoped YBa$_2$Cu$_3$O$_y$. Nature Phys. **9**, 79-83 (2013).

[22] Wu, T. *et al.* Magnetic-field-induced charge-stripe order in the high-temperature superconductor YBa$_2$Cu$_3$O$_y$. Nature **477**, 1919 (2011).

[23] Hinton, J. P. *et al.* A new collective mode in YBCO observed by time-domain reflectometry. Phys. Rev. B **88**, 060508 (2013).

[24] Karpinski, J., Kaldis, E., Jilek, E., Rusiecki, S. & Bucher, B. Bulk synthesis of the 81-K superconductor YBa$_2$Cu$_4$O$_8$ at high oxygen pressure. Nature **336**, 660-662 (1988).

[25] Bobowski, J. S. *et al.* Oxygen chain disorder as a weak-limit scatterer in YBa$_2$Cu$_3$O$_{6.50}$. Physica C **460-462**, 914-915 (2007).

[26] Blanco-Canosa, S. *et al.* Resonant x-ray scattering study of charge-density wave correlations in YBa$_2$Cu$_3$O$_{6+x}$. Phys. Rev. B **90**, 054513 (2014).

[27] Altarawneh, M. M., Mielke, C. H., Brooks, J. S., Proximity detector circuits: an alternative to tunnel diode oscil-

lators for contactless measurements in pulsed magnetic field environments. Rev. Sci. Instr. **80**, 066104 (2009).

[28] Yamaji, K. *et al*. On the angle dependence of the magnetoresistance in quasi-two dimensional organic superconductors. J. Phys. Soc. Jpn **58**, 1520-1523 (1989).

[29] Andersen, O. K., Liechtenstein, A. I., Jepsen, O. & Paulsen, F., LDA energy bands, low energy Hamiltonians, t', t'', $t_\perp(k)$ and $J_\perp$. J. Phys. Chem. Solids **56**, 1573-1591 (1995).

[30] Schoenberg, D. *Magnetic oscillations in metals*, (Cambridge University Press, Cambridge 1984).

[31] Sebastian, S. E. *et al*. Quantum oscillations from nodal bilayer magnetic breakdown in the underdoped high temperature superconductor $YBa_2Cu_3O_{6+x}$. Phys. Rev. Lett. **108**, 196403 (2012).

[32] Kivelson, S. A. *et al*. How to detect fluctuating stripes in the high-temperature superconductors. Rev. Mod. Phys. **75**, 1201 (2003).

[33] Nie, L. *et al*. Quenched disorder and vestigial nematicity in the pseudogap regime of the cuprates. Proc. Natl. Acad. Sci. **111**, 7980 (2014).

[34] Chockalingam, S. P. *et al*. Visualizing the Charge Density Wave Transition in $2H$-$NbSe_2$ in Real Space. Phys. Rev. B **89**, 235115 (2013).

[35] Fujita, K. *et al*. Direct phase-sensitive identification of a d-form factor density wave in underdoped cuprates. Proc. Natl. Acad. Sci. **111**, E3026 (2014).

[36] Le Tacon, M., Intense paramagnon excitations in a large family of high-temperature superconductors. Nature Phys. **7**, 725-730 (2011).

[37] Lee, P. A., Amperean Pairing and the Pseudogap Phase of Cuprate Superconductors. Phys. Rev. X **4**, 031017 (2014).

[38] Fradkin, E., Kivelson, S. A., Tranquada, J. M., Theory of Intertwined Orders in High Temperature Superconductors. http://arxiv.org/abs/1407.4480 (2014).

[39] Seo, K., Chen, H.-D., and Hu, J. d-wave checkerboard order in cuprates. Phys. Rev. B **76**, 020511(R) (2007).

[40] Efetov, K. B., Meier, H., Pépin, C., Pseudogap state near a quantum critical point. Nature Phys. **9**, 442-446 (2013).

[41] Pépin, C., de Carvalho, V. S., Kloss, T., Montiel, X. Pseudogap, charge order, and pairing density wave at the hot spots in cuprate superconductors. Phys. Rev. B **90**, 195207 (2014).